Review of Scientific Instruments

Opto-electro-modulated transient photovoltage and photocurrent system for investigation of charge transport and recombination in solar cells

Cite as: Rev. Sci. Instrum. **87**, 123107 (2016); https://doi.org/10.1063/1.4972104
Submitted: 27 April 2016 . Accepted: 29 November 2016 . Published Online: 20 December 2016

Jiangjian Shi, Dongmei Li, Yanhong Luo, Huijue Wu, and Qingbo Meng

Opto-electro-modulated transient photovoltage and photocurrent system for investigation of charge transport and recombination in solar cells

Jiangjian Shi,[1,2] Dongmei Li,[1,2] Yanhong Luo,[1,2] Huijue Wu,[1] and Qingbo Meng[1,2,a)]
[1]*Key Laboratory for Renewable Energy, Chinese Academy of Sciences, Beijing 100190, People's Republic of China and Beijing Key Laboratory for New Energy Materials and Devices, Institute of Physics, Chinese Academy of Sciences, Beijing 100190, People's Republic of China*
[2]*University of Chinese Academy of Sciences, Beijing 100049, People's Republic of China*

(Received 27 April 2016; accepted 29 November 2016; published online 20 December 2016)

An opto-electro-modulated transient photovoltage/photocurrent system has been developed to probe microscopic charge processes of a solar cell in its adjustable operating conditions. The reliability of this system is carefully determined by electric circuit simulations and experimental measurements. Using this system, the charge transport, recombination and storage properties of a conventional multicrystalline silicon solar cell under different steady-state bias voltages, and light illumination intensities are investigated. This system has also been applied to study the influence of the hole transport material layer on charge extraction and the microscopic charge processes behind the widely considered photoelectric hysteresis in perovskite solar cells. *Published by AIP Publishing.* [http://dx.doi.org/10.1063/1.4972104]

I. INTRODUCTION

Solar cells, based on semiconductor physics, have been developed for tens of years as a promising alternative to solve the increasingly serious energy and environmental problems.[1–3] Due to the mature material and device preparation technology, crystal silicon solar cells have achieved high efficiency and commercialization.[4,5] Nevertheless, there are ongoing efforts toward designing and developing efficient low-cost and environmentally friendly new-generation solar cells. Various materials, including inorganic semiconductors,[6,7] organic molecules and polymers,[8–10] hybrid semiconductors[11,12] and low-dimensional quantum dots and wells,[13–16] and device structures have been employed, which has created a large family of photovoltaic devices and complicated photoelectric systems.

In the cell, several processes including charge generation, separation, transport, extraction, collection, and recombination processes occur to produce electricity, which is common for most photoelectric systems.[2] These processes occur in the time scale ranging from femtoseconds to milliseconds. In particular cells, the charge also undergoes hysteresis in a longer time scale.[17] Aside from the time scale, these processes also occur in different spaces or regions inside the cell, such as the bulk and interfaces. According to the fundamental principles of charge conservation and continuity, the charge output and cell performance are determined by these processes.[2,18] The ultimate purpose of engineering the material, structure, and interfaces of the cell is to control and optimize these charge processes for high device performance. Thus, it is essential to establish a systematic understanding of these charge processes in different photoelectric systems to give purposeful guidelines for device design and optimization.

So far, some techniques have been developed to spatially and temporally probe the charge processes in various photoelectric systems. Femtosecond laser-based transient absorption[19–22] and terahertz photoconductivity[23,24] spectroscopies can probe the ultrafast charge generation, separation, and interfacial transfer processes. By measuring the AC current response of the cell to an AC voltage perturbation, the impedance spectroscopy can provide information on charge recombination based on equivalent device models.[25,26] Similarly, intensity-modulated photocurrent/photovoltage spectroscopy (IMPS/IMVS) is an AC perturbation measurement, which has been widely applied to investigate charge transport and recombination in sensitized solar cells.[27,28]

Compared to the above methods, the transient photocurrent (TPC) and photovoltage (TPV) method, based on short-pulse laser and high-speed electrical detection, has its distinctive advantage of directly measuring the charge transport and recombination in the time scale ranging from picoseconds to milliseconds for a practical cell; it has also been applied in the investigation of silicon,[29,30] quantum dots,[31] organic[32] and sensitized[33,34] solar cells or photodetectors. The theory for this measurement in sensitized solar cells was also established.[33] Simultaneously, efforts towards enhancing the measuring quality and capability have also been reported.[35–37] However, this method can only obtain the charge transport and recombination properties under short- and open-circuit conditions,[33] respectively. In fact, the short- or open-circuit condition is a type of extreme condition in solar cells, which is not applicable for general semiconductor devices; instead, the electric field or bias voltage is the essential physical quantity. Thus, more universal measuring methods and theories are needed. Realizing the probing of charge dynamics in experiment under modulation of the electric field and light illumination could provide more valuable information on the physical properties, operating mechanisms, and device performance of solar cells or other related photoelectric

a)Author to whom correspondence should be addressed. Electronic mail: qbmeng@iphy.ac.cn

devices. Although some voltage or current sources have been introduced to control the steady-state working conditions of solar cells,[31,38] probing the TPV properties of a solar cell under different electric fields remains a challenge.

In this work, an opto-electro-modulated TPV/TPC system (M-TPV/M-TPC) has been developed by designing the system structure and electric circuits to probe the charge processes of a solar cell under modulation of the electric field and light illumination. The measuring capability and reliability of this system are carefully monitored by electric circuit simulations and experimental testing. With this system, the microscopic charge transport, recombination, and storage properties of a commercial multicrystalline silicon solar cell are investigated. The influence of the hole transport material layer on the charge extraction and microscopic charge processes behind the widely considered photoelectric hysteresis in perovskite solar cells are also studied. Moreover, the influence of cell capacitance on TPC measurements is discussed, which demonstrates that the electrical transient system can accurately measure the total charge flow through the cell.

II. EXPERIMENT

A. Sample fabrication

The multicrystalline silicon solar cell was directly purchased from Stark Electronics, China. The perovskite solar cells used for the measurements were fabricated as previously described.[39] First, a dense TiO_2 compact layer with a thickness of approximately 50 nm was spin coated onto the pre-cleaned laser-patterned F-doped SnO_2 (FTO) glass and then sintered at 500 °C for 30 min. An (FA, MA)PbI_3 absorber film was deposited onto the TiO_2 layer using a repeated interdiffusion method. First, a 1.3M PbI_2 solution was spin coated at a speed of 4000 rpm and heated on a hot plate at 70 °C for 2 min, forming a transparent yellow film. After cooling down to room temperature, (FA, MA)I isopropanol solution (mole ratio FA: MA = 2:1) with a concentration of 30 mg/ml was repeatedly spin coated onto the PbI_2 film to form a smooth film. This film was then rinsed with isopropanol to remove the (FA, MA)I residual and heated at 120 °C for 100 min to completely transform the film into a transparent dark brown perovskite film. Spiro-OMeTAD was then spin coated onto the perovskite film as a hole transport material layer (HTM). For the HTM-free (HF) cell, no Spiro-OMeTAD was deposited. This FTO/TiO_2/perovskite/HTM film was kept overnight in the dark in air (humidity: 20%). Finally, Au was thermally evaporated (Kurt J. Lesker) as the back electrode (80 nm) at an atmospheric pressure of 10^{-7} Torr.

B. Experimental setup and measurements

The M-TPC/M-TPV system that we designed is shown in Figure 1(a). For the measurements, non-equilibrium carriers in the cell are excited by a 532 nm (Brio, 20 Hz, 4 ns) or 660 nm (CNI-laser, 1 kHz, 20 ns) pulse laser. A digital oscilloscope (Tektronix, DPO 7104) is used to record the photocurrent or photovoltage decay process with a sampling resistor of 50 Ω or 1 MΩ, respectively. It is worth noting that a much larger sampling resistance may be required to probe a much slower recombination dynamics. A white LED with a light intensity of 100 mW/cm^2 provides the bias illumination, and a high-speed

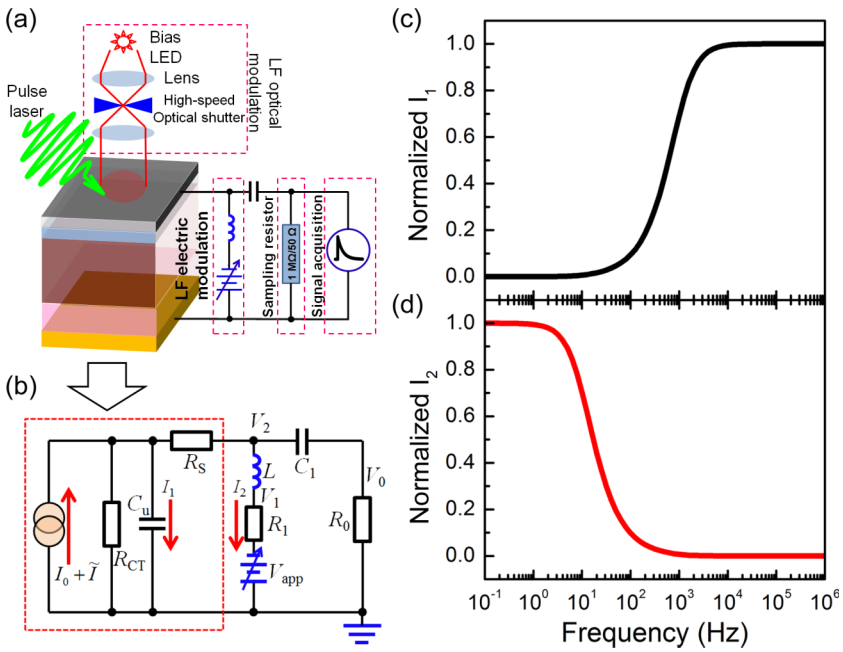

FIG. 1. (a) Schematic diagram of the designed M-TPC/M-TPV system. In detail, an electric circuit consisting of a digital signal generator and an inductor is connected in parallel to the cell to provide electrical modulation through the cell. A digital oscilloscope with a sampling resistance of 50 Ω or 1 MΩ is used to acquire the transient photocurrent or photovoltage signals produced by the pulse laser. An LED together with optical lenses and a high-speed shutter is used as the bias light source. (b) Equivalent electric circuit of the system and the measured cell. The cell is modeled as a parallel connection of a current source (I_0), a charge recombination resistance (R_{CT}), and a capacitance (C_u). R_s is the series resistance of the cell. V_{app} is the bias voltage from the signal generator and R_1 is the resistance of the electric modulation circuit. R_0 is the sampling resistance for signal acquisition. Simulated spectra for the AC current magnitude through the (c) capacitance (I_1) and (d) electrical modulation circuit (I_2).

optical shutter is used to control the on and off switching of the illumination. A digital signal generator (Tektronix, AFG 3052C) is used to provide an external modulation to the cell, which is connected in parallel to the signal acquisition circuit. A low-pass filter (LPF) with an inductor (for example, 50 H) and a capacitor (for example, 10 μF) is applied to separate the transient electrical signal from the voltage source to avoid shunting the output. The signal-filtering capability of the LPF can be adjusted to satisfy different measurement demands. Because of the LPF, the high-frequency TPC/TPV signals cannot pass through the electric modulation circuit but just evolve with their own dynamic behaviors. The DC resistance of this electric modulation circuit is low enough to allow the DC current from the cell to pass through, which prevents the development of a steady-state photovoltage. The DC or low-frequency electric modulation from the signal generator can also pass through the LPF and apply at the cell. Thus, the voltage applied at the cell is directly controlled by the signal generator and can be measured by a digital voltmeter. This instrument design with an electric circuit filter makes it possible to measure the TPC/TPV dynamics of a cell under certain bias voltages and illuminations. For all the measurements, the transient signals start recording 5 min after the external modulations are applied to avoid the possible influence of device response velocity, and the signals are averaged to obtain a reliable result. The pulse laser intensity, external bias voltage, and light illumination need to be adjusted to satisfy the perturbation demand of this method. For the undoped or only slightly doped semiconductor devices, a bias illumination or bias voltage may be required to produce a steady-state carrier distribution.

III. RESULTS AND DISCUSSION

A. Design principle, equivalent electric circuit, and reliability of the system

According to semiconductor physics, the steady-state charge transport in the absorber of a solar cell can be described as follows (take electrons as an example):[2,18]

$$D_n \frac{\partial^2 n}{\partial x^2} + \mu_n E \frac{\partial n}{\partial x} + n\mu_n \frac{\partial E}{\partial x} - \frac{(n - n_0)}{\tau_e} + G(x) = 0, \quad (1)$$

where D_n is the diffusion coefficient, n is the electron concentration, x is the position, μ_n is the mobility, E is the internal electric field, τ_e is the carrier lifetime, and G is the charge generation rate. In this physics model, the electric field and charge generation are independent basic working parameters of a solar cell, which are controlled by the external voltage and light illumination, respectively. The overall charge output and cell performance are determined by the steady-state boundary conditions of the cell. When a pulse perturbation is introduced into the transient measurement, the perturbation charge ($\tilde{n}$) transport can be derived as follows:

$$D_n \frac{\partial^2 \tilde{n}}{\partial x^2} + \mu_n E \frac{\partial \tilde{n}}{\partial x} + \tilde{n}\mu_n \frac{\partial E}{\partial x} - \frac{\tilde{n}}{\tau_e} + \tilde{G}(x) = \frac{\partial \tilde{n}}{\partial t}. \quad (2)$$

The charge transport or storage under the pulse perturbation would produce measurable TPC or TPV signals. Correspondingly, the TPC and TPV results can provide extremely valuable microscopic charge information about the cell. In the conventional method, the resistance of the signal acquisition circuit is used to control the boundary condition of both the steady-state and the transient charge transport. In the TPC measurement, the cell is always in the short-circuit condition; while in the TPV measurement, the cell is maintained in the open-circuit condition. This simple controlling method cannot keep the cell in its practical operating conditions when the electrical transient measurements are performed. The aim of our designed system is to solve this problem by independently controlling the boundary conditions of the steady-state and transient charge processes.

The equivalent electric circuit of the measurement system and the measured cell is shown in Figure 1(b), where the cell is modeled as a parallel connection of a current source (I_0), a charge recombination resistance (R_{CT}), and a cell capacitance (C_u). In this circuit, V_0 is the voltage signal that is measured by the oscilloscope, V_1 is the voltage from the signal generator, and V_2 is the total voltage applied at the cell. When measuring the photovoltage decay process, a large sampling resistance is used. Thus, the photoinduced pulse charge ($\tilde{I}$) may pass through two different routes, as shown with I_1 and I_2 in Figure 1(b). When the charge flows into the cell capacitor, it will be stored to generate the photovoltage, and then it decays through recombination processes. If the charge passes through the electric modulation circuit, as I_2 does, it is a shunt loss, which can accelerate the photovoltage decay process and affect the measurement accuracy. Figures 1(c) and 1(d) give the AC magnitude spectra of I_1 and I_2, respectively. Low-frequency current mainly passes through the electric modulation circuit (i.e., the signal generator). For high-frequency current, the pulse charge would be stored in the cell capacitor. In most of the transient measurements, the perturbation charge is excited by a short-pulse laser with duration of about several nanoseconds and is transported through the cell within microseconds, which is typical for high-frequency signals. Thus, the pulse charge would be stored and recombined within the cell to generate the TPV.

Figure 2(a) gives the simulated transient voltage signal at different points of the equivalent electric circuit in Figure 1(b) after a pulse charge injection of 0.3 nC, where R_{CT} = 5 kΩ, C_u = 30 nF, and a DC bias voltage of approximately 0.1 V is provided by the voltage source. As observed, V_1 exhibits a constant voltage of approximately 97 mV, which indicates that no transient charge passes through this point and only a small DC bias voltage is shared by the resistance of the electric modulation circuit. The total voltage applied at the cell shows an exponential decay and yields a lifetime of approximately 150 μs, which agrees well with the device model by following the equation $\Delta V = \Delta V_0 \exp[-t/(R_{CT}C_u)]$. The TPV would also be applied at the cell, but it has little influence on the electric properties of the cell because it is much smaller than the DC bias voltage. After coupling with the capacitance of C_1, the high-frequency TPV is recorded by the digital oscilloscope as V_0. The shape of the V_0 decay is the same as that of V_2, which indicates that an accurate measurement of the photovoltage decay process was conducted.

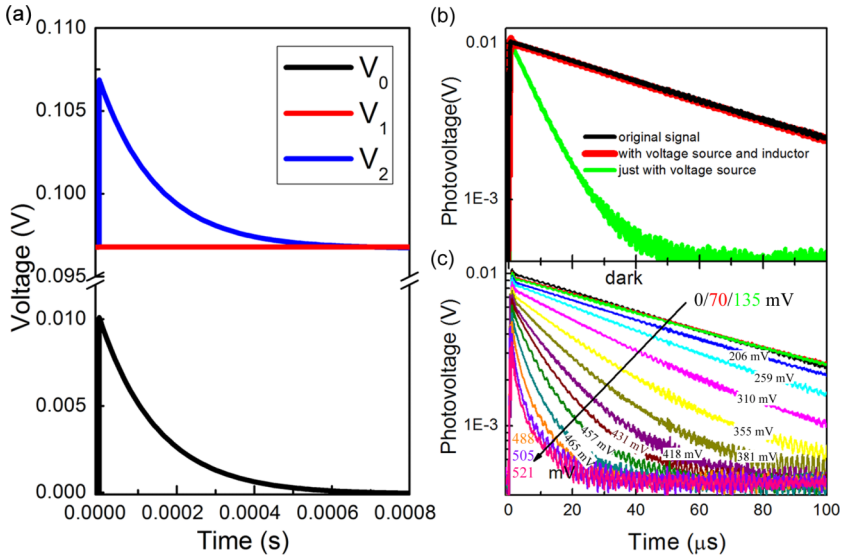

FIG. 2. (a) Simulated transient voltage signals at different points of the equivalent electric circuit, where V_2 is the total voltage applied at the cell, V_1 is the bias voltage from the signal generator, and V_0 is the voltage signal recorded by the oscilloscope. Experimentally measured transient photovoltage signals of a multicrystalline silicon solar cell in different conditions ((b) measured with different measuring electric circuits and (c) under different steady-state bias voltages ranging from 0 to 521 mV in the dark).

To confirm this result in experiments, the TPV of a multicrystalline silicon solar cell was measured, as shown in Figure 2(b). First, a conventional system without the electric modulation circuit was used to obtain the original signal. Our system was also used to measure the TPV in the dark and under zero bias voltage, which gives the same signal as the original one. However, without the LPF, the photovoltage signal is obviously shunted. Clearly, this system with the LPF is reliable. More comparisons between these two methods are shown in the supplementary material, where an illumination-sensitive perovskite solar cell is used as the sample. Furthermore, the photovoltage decay properties of the silicon solar cell under different DC bias voltages ranging from 0 to 521 mV are measured, as shown in Figure 2(c). For all these photovoltage signals, the primary part of the curve exhibits a single exponential decay behavior, which agrees with the device model in Figure 1(b). When the bias voltage is increased, both the peak photovoltage and the decay lifetime are decreased, which implies an enhanced charge recombination process.

In Secs. III B–III E, based on the confirmed reliability, we will present a systematic discussion on the microscopic charge processes and physical quantities of a solar cell measured by this system. As examples, the charge extraction, collection and quantum efficiencies, charge recombination dynamics, charge storage, and slow charge response in the silicon or perovskite solar cells will be presented. For clarity, the physics models for the measurement and analysis are discussed in the supplementary material.

B. Charge extraction, collection, and quantum efficiencies

Here, we will show that the charge extraction, collection, and quantum efficiencies of a solar cell in its practical operating conditions, which are usually difficult to obtain by other methods, can be measured by the M-TPC and M-TPV methods. A commercial multicrystalline silicon solar cell is used as an example; the steady-state current–voltage (I-V) curve of this cell is shown in Figure 3(a). The TPC and TPV of this cell under different bias voltages and light illumination of 100 mW cm^{-2} are measured, as shown in Figures 3(b) and 3(c). These measurements have never been reported before, and neither the TPC nor the TPV shown here can be measured using the conventional methods. For the TPC signals, the primary part exhibits a single exponential decay behavior, which agrees well with the discussions in the supplementary material. A single-exponential approximation can be employed to describe the decay dynamics of the TPC results. The cell has a TPC decay time (τ_C) of about 10 μs in the short-circuit condition. For this cell, the photoinduced free carriers have to experience lateral transport processes within the silicon layer; thus, a relatively long time is required for them to be collected by the grid-line metal electrodes. When the bias voltage is increased, the peak photocurrent and the decay time are clearly decreased. For the TPV, a recombination lifetime (τ_r) of approximately 70 μs at 0 mV is obtained. From the τ_C and τ_r, the effective charge collection time (τ_j) can also be obtained, which will be discussed further in Sec. III C. More details are provided in the supplementary material.

With these dynamics parameters, the microscopic charge processes including the interfacial charge extraction and collection and quantum efficiencies can be described, as shown in Figure 3(d). By integrating the TPC signals, the incident photon-to-electron conversion efficiency is obtained. The external quantum efficiency (EQE) of the cell at different bias voltages can be derived as N_e/N_0, where N_e is the total collected carriers and N_0 is the total incident photons. As observed in Figure 3(d), the EQE at 0 mV is approximately 87%, and it gradually decreases at higher bias voltages, which is a similar evolution behavior to the I-V curve. The charge collection efficiency (η_C) is calculated as

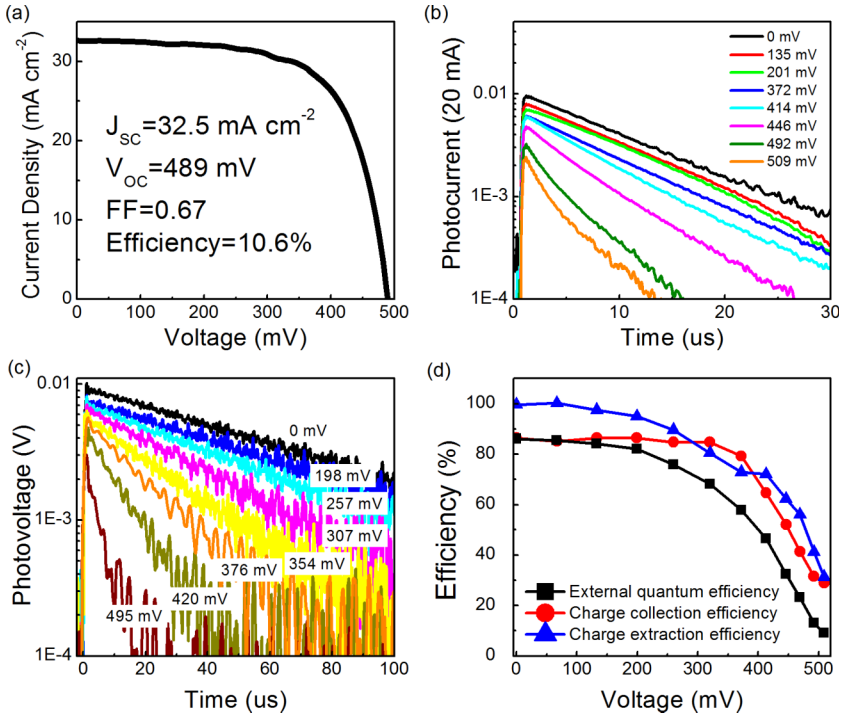

FIG. 3. (a) Steady-state current–voltage curve of a commercial multicrystalline silicon solar cell. (b) Transient photocurrent and (c) photovoltage curves of this cell under different steady-state bias voltages and a steady-state illumination of 100 mW cm^{-2}, respectively. (d) The extraction, collection, and photoelectric conversion efficiencies of the photoinduced charge at different bias voltages.

$1 - (\tau_j/\tau_r)/(1 + \tau_j/\tau_r)$. It can be observed that the η_C clearly decreases when the bias voltage is higher than 400 mV due to the increase in interfacial charge recombination at high voltages. Furthermore, the interfacial charge extraction efficiency (η_E) can be derived from the EQE and η_C, that is, $\eta_E = EQE/\eta_C$, as shown in Figure 3(d). The η_E is the ratio between the charge extracted from the *p*-type absorber into the n^+ layer and the total photoinduced charge. In this cell, there is negligible reflection from the incident 532 nm laser. The η_E also decreases at high voltages, which indicates that the bias voltages can influence the charge transport and recombination dynamics in the bulk absorber. These efficiencies are very important in describing the performance of a solar cell, and they can be applied to more accurately analyze the microscopic physical origins of differences in the device performance. However, it is difficult to obtain the η_C and η_E by other methods, especially in the operating conditions. Thus, this demonstrates the significance of the modulated electrical transient methods described here.

Furthermore, this system is used to investigate the perovskite solar cell. In this cell, an organic HTM layer is usually included for a higher efficiency. It is generally believed that this layer would help to transport photoinduced holes and to suppress charge recombination. However, TPV and impedance spectra measurements under illumination have shown that the charge recombination rates of the cells with or without the HTM layer are similar. Thus, the critical role of this HTM layer needs to be further clarified. Figure 4 presents the TPC of the cells with and without the HTM layer under different bias voltages. Two pulse lasers with wavelengths of 532 and 660 nm were used to excite the cell. For the cell with the HTM, the photocurrent decay time is approximately 3.5 μs under the short-circuit condition, which is obviously longer than that of the cell without a HTM layer. This result indicates that the introduction of a low-mobility organic HTM layer would slow down the charge transport. On the other hand, for the cell with the HTM, positive photocurrents are always observed regardless of the bias voltage or excitation wavelength. However, for the cell without the HTM, negative photocurrents can be easily observed when the bias voltages increase. When the free carriers are excited in the deep region close to the metal back electrode of the cell by a 660 nm laser, this negative signal can be observed for bias voltages as low as 600 mV.

From the M-TPC results, the η_E and η_C are derived, as shown in Figures 4(e) and 4(f). It can be observed that the η_E of the HTM-free cell is obviously lower than that of the cell with a HTM layer, especially when the free carriers are excited close to the back electrode and at high bias voltages. Since the electrons have to travel for a longer distance to be extracted by the TiO_2 layer while the transport distance for holes is much shorter when they are produced in the deep region, the lower η_E (HF-660 nm) can be attributed to the reduction in electron extraction. In the cell without a HTM layer, further calculations find that the photoinduced electrons, especially those in the deep region of the perovskite absorber, can travel towards both the front and the back contact layers. In the HTM-based cell, this transport of free electrons towards the back electrode is blocked, thus preventing the loss in effective charge extraction. The difference in the boundary conditions of charge transport in the perovskite absorber may be the physical origin for the difference in performance between the cells with and without the HTM layer. For the η_C, both cells are similar to each other. Therefore, the M-TPC measurements

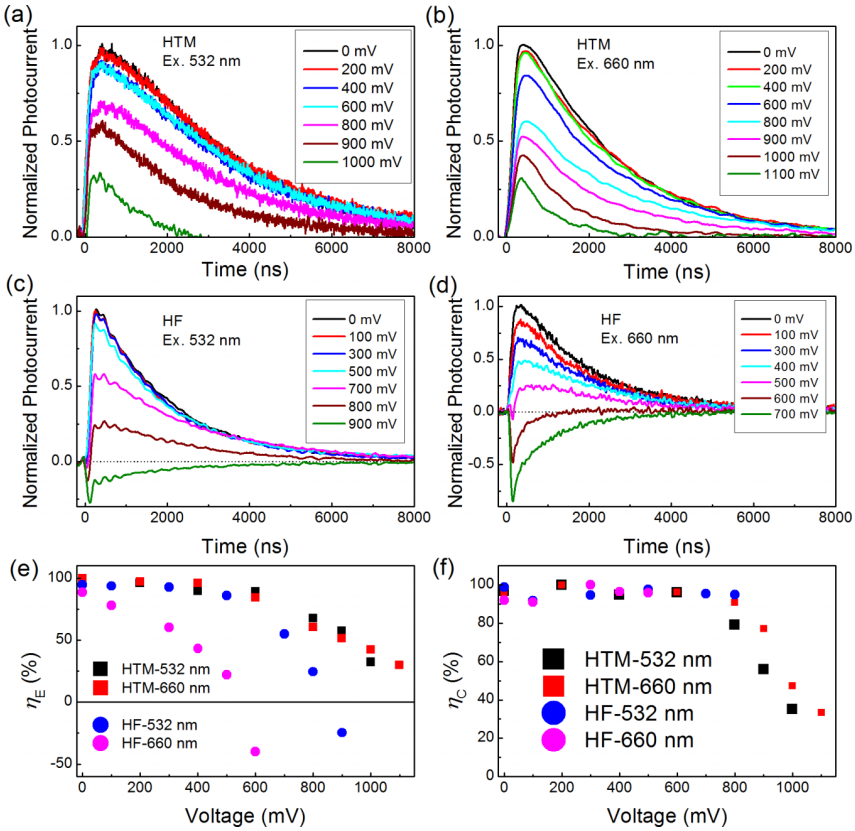

FIG. 4. Transient photocurrent results of the perovskite solar cells with or without a HTM layer under different steady-state bias voltages in the dark. The pulse lasers with wavelengths of 532 nm and 660 nm are applied as the excitation source. (a) With HTM 532 nm, (b) with HTM 660 nm, (c) without HTM 532 nm, (d) without HTM 660 nm, (e) charge extraction efficiency (η_E), and (f) collection efficiency (η_C) of the cells with and without an HTM layer. The negative η_E means that photoinduced electrons are transported toward the back electrode.

indicate that the HTM layer in the perovskite solar cell plays an important role in blocking the transport of photoinduced electrons towards the back electrode, which improves the electron extraction.

C. Recombination dynamics

The interfacial recombination rate ($k_r = 1/\tau_r$) of a solar cell is also an important physical quantity that affects the device performance; it is usually measured by the TPV method. However, it is difficult to measure the TPV of a cell at different bias voltages (not open-circuit conditions) without the modulation design presented in this work. Here, we will show that the k_r can also be measured with the TPC methods, as $k_r = 1/\tau_C - 1/\tau_j$. Detailed discussions are presented in the supplementary material. Figure 5(a) shows the decay time of the TPC and TPV of the silicon cell at different bias voltages in the dark and under illumination. The τ_j is calculated as approximately 11.8 μs, which is slightly larger than the τ_C. Figure 5(b) gives the k_r results of the cell calculated from the TPV and the TPC dynamics parameters. It can be observed that the results derived from the TPC method are similar to those from the universal TPV method, which demonstrates the rationalization for this method and the dynamics model we established. The k_r increases at higher voltages with an exponential relationship, which is probably due to the increase in the majority hole density at the interface for the recombination of non-equilibrium electrons.

D. Charge storage and differential capacitance

In addition to directly observing the charge transport and recombination decay behaviors, the charge storage and differential capacitance related to the carrier properties of the cell can also be measured. When the cell works, the non-equilibrium charge, which is stored in the cell, is an important physical quantity that is related to the junction property, defect characteristics, and device performance. This measurement was previously carried out with a charge extraction method and was usually performed under open-circuit conditions.[33] Here, we show that it can also be easily measured with the modulated electrical transient system. As an example, Figure 6(a) shows the density of the non-equilibrium charge stored in a working silicon solar cell at a certain bias voltage with and without the light illumination. The non-equilibrium charge is obtained by measuring the current decay when the bias voltage and light illumination over the cell are simultaneously switched off within 500 ns. It is found that both the bias voltage and light illumination can influence the stored charge. Interestingly, the relationship between the stored charge and the bias voltage can be well fitted with a depleted n^+-p junction model, where the measured non-equilibrium charge can be described as $\sqrt{2\varepsilon_s N\varphi_{bi}}\left(1-\sqrt{1-V/\varphi_{bi}}\right)$. The fitting results give a built-in potential (V_{bi}) of approximately 0.56 V and a hole density of approximately 1.5×10^{16} cm^{-3}. This hole density is similar to that measured by the AC capacitance method, although a slight difference in the V_{bi} exists. For the charges measured under

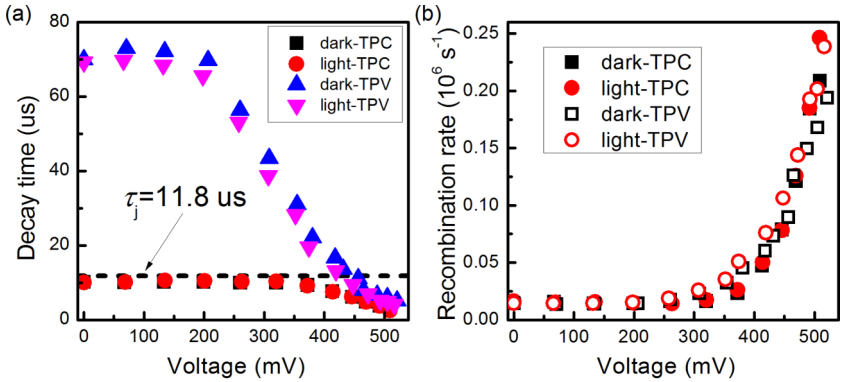

FIG. 5. (a) The decay time of the photocurrent and photovoltage of the silicon solar cell and (b) the recombination rate of the cell, which are derived from the M-TPC and M-TPV results.

illumination, the density of the additional carriers produced by the illumination is estimated to be approximately 10^{12} cm^{-3} in the short-circuit condition, which is much lower than 10^{16} cm^{-3}. Thus, it is inferred that the light illumination does not obviously influence the junction property of the silicon solar cell, whose thickness is about hundreds of micrometers. Along with the measured charge, the capacitance of the cell can be derived by differential calculations. The Mott-Schottky curves are shown in Figure 6(b). A linear relationship is observed between $1/C^2$ and the bias voltage, which further confirms the discussions above.

The charge storage properties of the selective charge extraction layer (SCEL, e.g., TiO_2 in the perovskite solar cell or n^+ Si in the silicon cell) can also be measured with the M-TPC and M-TPV methods. In a solar cell, the photoinduced charges in the absorber would be extracted into the SCEL. Under the short-circuit condition, these charges are transported through the SCEL and the external electric circuit to produce the TPC; while under the open-circuit condition, they are extracted and stored in the SCEL to generate an additional photovoltage (ΔV), and then they decay due to the recombination. With the ΔV and the corresponding total extraction charge (ΔQ_0), the differential capacitance (C) of the SCEL can be derived as $C = \Delta Q_0/\Delta V$. For example, Figure 7(a) presents the total collected charge (ΔQ_C) obtained by directly integrating the TPC signals, the ΔQ_0 calculated with equation (supplementary material), and the ΔV. In the conventional TPC and TPV methods for sensitized solar cells, the ΔQ_0 was usually considered as a constant.[33] However, our experimental results based on the planar perovskite and silicon solar cell show that the charge extraction is undeniably dependent on the bias voltage. The ΔQ_0 decreases slightly when the bias voltage is increased from 0 to approximately 800 mV, and it significantly decreases by approximately 5 to 6 times at higher voltages. The ΔQ_C reduction is more obvious due to the decrease in η_C at high bias voltages. Similarly, the ΔV decreases at high voltages. Clearly, these decreases cannot be attributed to the measurement errors. In the conventional method, the decrease in ΔV is usually attributed to the increase in capacitance at high voltages. However, our experiments may provide a different result.

With the ΔQ and ΔV, the differential capacitance is deduced, as shown in Figure 7(b). Here, the capacitance is calculated as $C = \Delta Q$ (V)/ΔV (V) or $C = \Delta Q$ (0 V)/ΔV (V). The latter has been widely used in sensitized solar cells.[33,34] The calculated differential capacitance increases gradually when the bias voltage is higher than 800 mV. However, in the semiconductor junction-based solar cell, the free carriers have to first experience transport and recombination processes before they are injected into the SCEL. In this case, the extracted charges should be bias voltage-dependent, as shown in Figure 7(a). Considering this condition, the

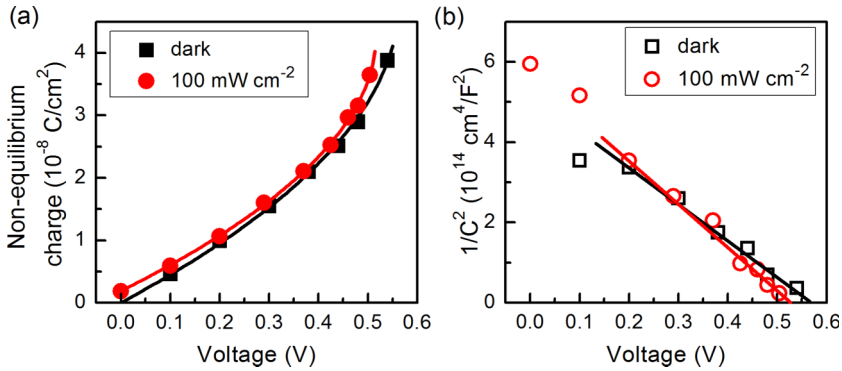

FIG. 6. (a) The non-equilibrium charge stored in the working silicon solar cell at a certain bias voltage with or without the light illumination. The results are fitted using a depleted n^+-p junction model. (b) Mott-Schottky curves of the cells, where the capacitance is derived from the non-equilibrium charge. The solid lines are guides for the eyes. The non-equilibrium charge was obtained by measuring the current decay when the bias voltage and light illumination applied at the cell are simultaneously switched off within 500 ns.

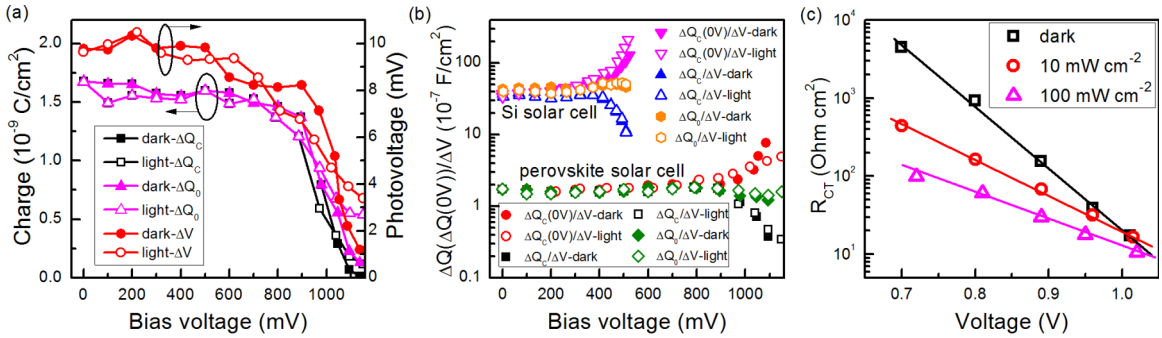

FIG. 7. (a) Total extracted (ΔQ_0) and collected (ΔQ_C) photoinduced charge and peak photovoltage (ΔV) of a planar perovskite solar cell. (b) Differential capacitance of the silicon and perovskite solar cell under different bias voltages in the dark and under steady-state light illumination of 100 mW cm^{-2}. (c) Charge recombination resistance (R_{CT}) of the perovskite solar cell at different bias voltages in the dark and under illumination (10 and 100 mW cm^{-2}). The solid lines are the exponential fits of R_{CT} vs. voltage.

differential capacitance is re-calculated as ΔQ_0 (V)/ΔV (V), as indicated by the green square in Figure 7(b). The capacitance remains almost constant with a value of approximately 1.5×10^{-7} F/cm^2 at the bias voltages ranging from 0 to 1150 mV. This phenomenon is also observed in the silicon solar cell. Thus, it can be inferred that the bias voltage is not applied at the TiO_2 layer but at the perovskite absorber. If the photoinduced charge is mainly stored in the conduction band of the TiO_2 layer, the capacitance can be derived as $q^2 N_C / K_B T \times \exp[(E_C - E_F)/K_B T]$, where q is the electron charge, N_C is the effective density of states of the conduction band, K_B is the Boltzmann constant, T is the temperature, E_C is the energy level of the conduction band minimum, and E_F is the Fermi energy level. With the constant capacitance of 1.5×10^{-7} F/cm^2, the density of the majority electron carriers in the TiO_2 compact layer (thickness of 10 nm) in this cell can be estimated as approximately 2.8×10^{16} cm^{-3}. Under illumination, the same result is obtained, which means that the illumination does not affect the carrier occupancy properties of the TiO_2 layer. The theoretical simulations based on a junction device model also support the conclusion that the bias voltage or light illumination does not change the carrier properties of the n-TiO_2 layer. This constant capacitance is different from that in the sensitized solar cell, which may be due to the obvious distinctions in the charge transport process inside the cell and the interfacial charge extraction velocity.[40] However, the influence of the bias voltage on the charge extraction in sensitized solar cells is still uncertain.[41] Thus, an accurate measurement of the total extracted charge at different bias voltages, not only under the short-circuit condition, is required to obtain a more reliable result. The ΔQ_C is also used to calculate the capacitance, which gives a lower value at high voltages. This is probably due to the imperfect collection of charges that produce the photovoltage due to the interfacial recombination.

Moreover, the R_{CT} of the cell, which is a widely used physical quantity to describe the interfacial recombination and is usually obtained by the impedance spectra (IS), can also be obtained by the M-TPC and M-TPV methods. According to the discussions in Section III A, it can be derived as $R_{CT} = \tau_r / C$. Using the TPV decay time and the C, the R_{CT}s of the perovskite solar cell at different bias voltages in the dark and under illumination (10 and 100 mW cm^{-2}) are calculated and shown in Figure 7(c). An exponential relationship is found between the R_{CT} and the bias voltage regardless of the illumination conditions, which agrees well with the general charge transfer model of a junction solar cell and the IS results.[40] Under the dark condition, the exponential fit gives an ideality factor (A) of approximately 2.1 and an inverse saturated current density (J_0) of approximately 3.07×10^{-8} mA cm^{-2}. Interestingly, the A is increased to 3.7 and 5.0 under light illumination of 10 mW cm^{-2} and 100 mW cm^{-2}, respectively. This phenomenon is also observed in the I-V and IS measurements, which may indicate that the relation between free carrier density and the bias voltage in the perovskite solar cell is dependent on illumination conditions.

E. Pulse-voltage modulation to probe photoelectric hysteresis processes in perovskite solar cells

The sections above mainly show the steady-state modulation methods used to investigate charge transport and recombination of a solar cell. Moreover, the transition-state properties of a solar cell may exhibit more interesting behaviors. Recently, the observation of an anomalous photoelectric hysteresis in perovskite solar cells has attracted wide interest.[17,42–46] This hysteresis means that the current–voltage characteristics of the cell are significantly dependent on the measurement conditions, such as the scanning rate and pre-bias conditions. Many efforts have been made to clarify its origins, which have resulted in various interpretations and ongoing debates.[43–46] Due to the advantages of easy modulation of the operating states and high-speed signal acquisition, the electrical transient method described in this work is also an effective approach for *in situ* observation of the microscopic charge processes behind the macroscopic hysteresis behavior in this cell.

Figure 8(a) depicts the *in situ* measurement of the transient charge processes under pulse-electrical modulations with this system. When the external applied electric field (E_a) at the cell is switched rapidly, the internal electric field inside the cell produces a response. During the duration of this response, exciting the cell with a short-pulse laser at different times and probing the charge transport or recombination can produce important information about the evolution of this internal electric field. This *in situ* measurement demands that

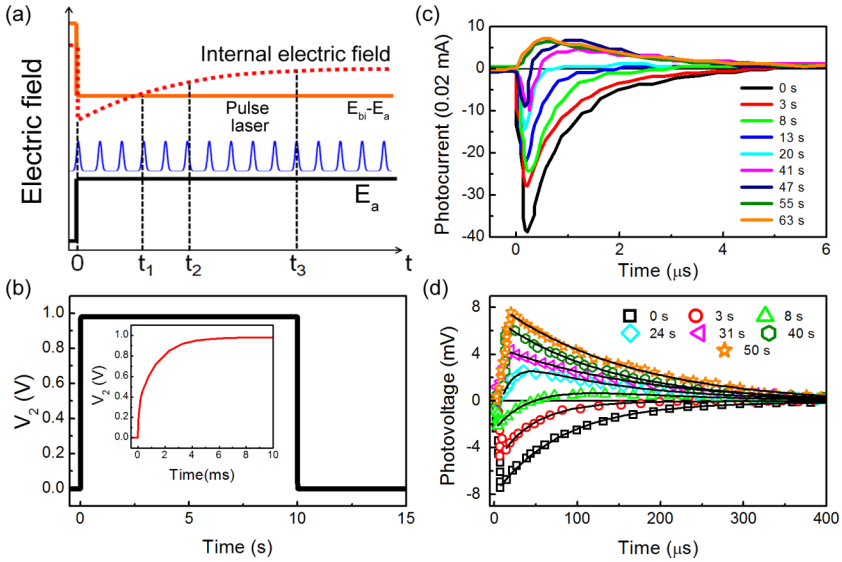

FIG. 8. (a) Schematic diagram of the *in situ* measurement of the transient charge processes under pulse-electrical modulations, where E_a is the pulse bias electric field from the external modulation and E_{bi} is the junction built-in electric field. (b) The voltage applied at the cell when the signal generator generates a pulse electrical modulation (inset: magnified rise stage of the pulse voltage signal). (c) Transient photocurrent (0–900 mV) and (d) photovoltage (0–800 mV) at different times after the bias voltage at the cell is switched. The photovoltage is fitted with exponential decay equations.

the switching time of the E_a should be much shorter than the response time of the internal electric field in the cell. Figure 8(b) shows the change of V_2 when a pulse voltage of approximately 1 V is generated from the signal generator. The rise time of the original pulse signal is approximately 10 ns. Due to the low-pass inductance, the rise time is prolonged to approximately 10 ms, as shown in the inset in Figure 8(b), which is still much shorter than the hysteresis time in seconds.

The planar perovskite solar cell with significant hysteresis is used as the sample. Figure 8(c) shows the TPC results of the cell at different times after the bias voltage is switched from 0 to 900 mV. In the early stage, a high negative photocurrent is observed. The absolute value of this negative signal gradually decreases with time. At the time of approximately 20 s, a small positive shoulder appears after the decay of a negative peak. Afterwards, the negative peak decreases continuously and the positive shoulder increases. At the time of approximately 55 s, only a positive photocurrent can be observed. According to our previous work, this slow evolution can be attributed to the migration of ions in the cell, which is driven by multiple electric fields.[47,48] In addition to the photocurrent, the *in situ* TPV can also be applied to reflect the evolution of electric properties of the cell. Figure 8(d) presents the TPV results of the cell at different times after the bias voltage is switched from 0 to 800 mV. Similar to the photocurrent results, the photovoltage also shows a negative value in the early stage, and then it gradually increases to positive values. At the early times of 0 and 3 s and the later times of approximately 31, 40, and 50 s, the TPV curves can be well fitted with a single exponential equation. Interestingly, in the intermediate stage of approximately 8 and 24 s, a double exponential equation is required to fit the photovoltage decay process. These time dependent microscopic behaviors can help to clarify the physical origins of the hysteresis with deeper theoretical investigations.

F. Influence of cell capacitance on electrical transient measurements

In the electrical transient measurement, the cell capacitance is always a factor due to its influence on the measurement accuracy of TPC during its charging and discharging processes.[49] Here, this influence on the photocurrent decay process will be discussed. First, the magnitude and phase of the measured photocurrents are simulated according to the equivalent electric circuit in Figure 1(b). Different cell capacitances (C_u = 1, 5, and 20 nF) and a sampling resistance (R_0) of 50 Ω are considered. The simulation results are shown in Figures 9(a) and 9(b). When C_u = 1 nF, the cut-off frequency can reach 3×10^6 Hz. Below this frequency, the signal phase is approximately 0°, which means that the TPC in the sub-microsecond and longer time scales can be accurately measured. For C_u = 5 nF, the cut-off frequency decreases to 6×10^5 Hz, which affords the accurate measurement of the microsecond photocurrent transients. When the C_u is further increased to 20 nF, the cut-off frequency is only approximately 1×10^5 Hz. In this case, the measured TPC with a decay time of several microseconds may more or less include measurement errors. This error comes from the charge and discharge processes of the cell capacitance. According to the equivalent electric circuit in Figure 1(b), the relationship between the actual photocurrent through the cell (i_C) and the measured photocurrent (i_m) can be derived as follows:

$$i_C(t) = i_m(t) + C_u(R_0 + R_S)\, i_m(t), \tag{3}$$

where R_S is the series resistance of the cell. With this equation, the i_C can be recovered when there are errors in the measurement of i_m. This has been demonstrated by Kettlitz *et al.*[49]

To more clearly observe this influence, the TPC is simulated based on the equivalent electric circuit, as shown in Figure 9(c). The original signal decays with a time of

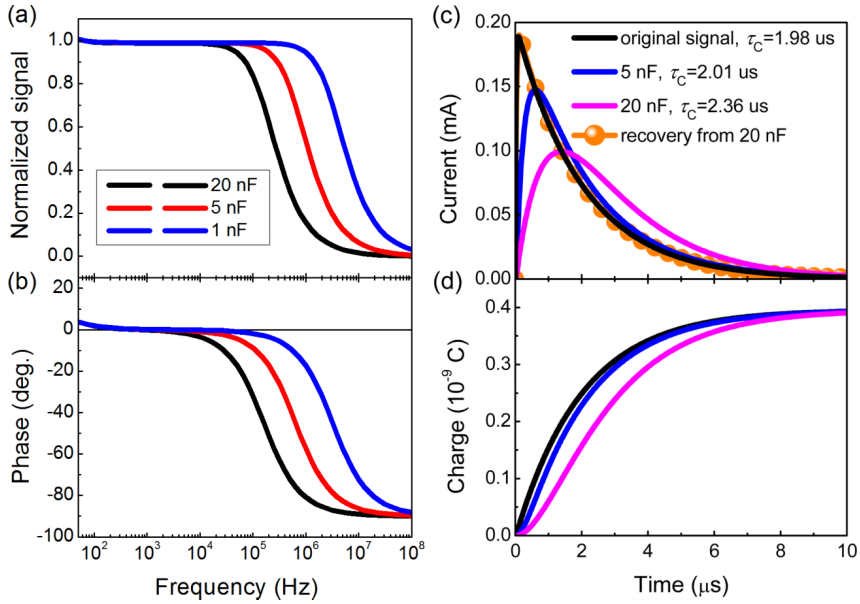

FIG. 9. Simulated AC spectroscopy of the (a) magnitude and (b) phase of measured photocurrent with different cell capacitances (1, 5, and 20 nF). (c) Simulated transient photocurrent signals of the cells with different capacitances and the recovered signal from the cell with a 20 nF capacitance. (d) The collected charge obtained by integrating the transient photocurrents.

1.98 μs, and the cell with C_u = 1 nF presents the same signal (not shown). For C_u = 5 nF, both the rise and fall processes are slowed down, which is accompanied with a decrease in the peak value. However, a similar τ_C of approximately 2.01 μs is still obtained. For C_u = 20 nF, these differences are more obvious, yielding a τ_C of approximately 2.36 μs and introducing a measurement error of approximately 19%. As shown in Figures 3 and 4, the TPC signals rise rapidly in our experiments, which implies that the TPC dynamics is not obviously influenced by the cell capacitance. Thus, we believe that the dynamic parameters of the TPC results used in the above sections are reasonable, with negligible errors. According to Equation (3), the transient signal is recovered, and it yields the same signal as the original one. Thus, to obtain accurate information about the charge transport velocity, the influence of the capacitance should be considered to avoid significant errors, and the TPC signal can be recovered. It is worth noting that although the cell capacitance can affect the measured TPC behavior, it cannot change the direction of the photocurrent. Thus, the hysteresis shown in Figure 8 should not be attributed to the capacitance effect.

Here, we will further demonstrate that the capacitance does not affect the accurate measurement of the collected charge by the TPC method. The collected charge of the cell can be obtained by integrating the photocurrent,

$$\begin{aligned} Q_C &= \int_0^{t_0} i_C(t)\,dt = \int_0^{t_0} i_m(t) + C_u(R_0+R_S)\,i_m(t)\,dt \\ &= \int_0^{t_0} i_m(t)\,dt + \int_0^{t_0} C_u(R_0+R_S)\,i_m(t)\,dt \\ &= Q_m + C_u(R_0+R_S)\,i_m|_0^{t_0}. \end{aligned} \tag{4}$$

In this equation, the parameters 0 and t_0 are the lower and upper time limits of the photocurrent decay process. For a complete TPC signal, $i_m(0) = i_m(t_0) = 0$. Thus, the right side of Equation (4) can be further calculated as Q_m, that is, $Q_C = Q_m$. For clarity, the current signals shown in Figure 9(c) are integrated from 0 to 10 μs; the integrated results are shown in Figure 9(d). The rise behaviors under different C_u values are different, but they lead to the same total charge value. Based on this result, the charge measurement with the TPC method is reliable.

IV. CONCLUSION

An M-TPC/M-TPV system has been developed. With this system, the microscopic charge transport, recombination, and storage properties of a solar cell can be accurately probed under modulation of the electric field and light illumination. The capability and reliability of this system are carefully determined by electric circuit simulations and experimental comparisons. This system exhibits extraordinary advantages over the conventional TPC/TPV method; in particular, it can quantitatively investigate the charge extraction and collection efficiency at the interfaces of a cell under its practical operating conditions. Moreover, this system provides more reasonable measurements of the charge storage properties of the cell and the carrier density in the semiconductor absorber and in the SCEL. Moreover, we present a method of obtaining the charge recombination rates by the TPC measurements. Finally, it also has distinct advantages in probing the microscopic charge processes behind the macroscopic hysteresis observed in perovskite solar cells by an *in situ* measurement, which may provide important experimental evidence for clarifying the physical mechanisms behind hysteresis. Thus, this modulated electrical transient method can be an impactful experimental technique for investigating general and specific charge processes in various photoelectric systems.

SUPPLEMENTARY MATERIAL

See supplementary material for the physics models for the measurement and analysis and more comparisons between the conventional and M-TPC/M-TPV methods.

ACKNOWLEDGMENTS

This work was supported by the Natural Science Foundation of China (Grant Nos. 51372270, 11474333, 51421002, 91433205, and 51627803).

[1]S. G. Benka, Phys. Today **55**(4), 38 (2002).
[2]A. Luque and S. Hegedus, *Handbook of Photovoltaic Science and Engineering* (John Wiley & Sons, UK, 2011).
[3]A. Polman, M. Knight, E. C. Garnett, B. Ehrler, and W. C. Sinke, Science **352**, 307 (2016).
[4]See http://www.nrel.gov/ncpv/images/efficiency_chart.jpg for NREL, Best research cell efficiency; accessed April, 2016.
[5]M. A. Green, K. Emery, Y. Hishikawa, W. Warta, and E. D. Dunlop, Prog. Photovoltaics: Res. Appl. **22**, 701 (2014).
[6]S. Wager, J. L. Shay, P. Migliorato, and H. M. Kasper, Appl. Phys. Lett. **25**, 434 (1974).
[7]D. A. Cusano, Solid State Electron. **6**, 217 (1963).
[8]C. W. Tang, Appl. Phys. Lett. **48**, 183 (1986).
[9]G. Li, V. Shrotriya, J. Huang, Y. Yao, T. Moriarty, K. Emery, and Y. Yang, Nat. Mater. **4**, 864 (2005).
[10]B. C. O'Regan and M. Grätzel, Nature **353**, 737 (1991).
[11]A. Kojima, K. Teshima, Y. Shirai, and T. Miyasaka, J. Am. Chem. Soc. **131**, 6050 (2009).
[12]C. R. Kagan, D. B. Mitzi, and C. D. Dimitrakopoulos, Science **286**, 945 (1999).
[13]A. J. Nozik, Phys. E **14**, 115 (2002).
[14]S. A. McDonald, G. Konstantatos, S. G. Zhang, P. W. Cyr, E. J. D. Klem, L. Levina, and E. H. Sargent, Nat. Mater. **4**, 138 (2005).
[15]P. V. Kamat, J. Phys. Chem. C **112**, 18737 (2008).
[16]K. W. J. Barnham and G. Duggan, J. Appl. Phys. **67**, 3490 (1990).
[17]H. J. Snaith, A. Abate, J. M. Ball, G. E. Eperon, T. Leijtens, N. K. Noel, S. D. Stranks, J. T.-W. Wang, K. Wojciechowski, and W. Zhang, J. Phys. Chem. Lett. **5**, 1511 (2014).
[18]S. M. Sze and K. K. Ng, *Physics of Semiconductor Devices* (Wiley, New York, 2006).
[19]G. Xing, N. Mathews, S. Sun, S. Lim, Y. M. Lam, M. Grätzel, S. Mhaisalkar, and T. C. Sum, Science **342**, 344 (2013).
[20]S. D. Stranks, G. E. Eperon, G. Grancini, C. Menelaou, M. J. Alcocer, T. Leijtens, L. M. Herz, A. Petrozza, and H. J. Snaith, Science **342**, 341 (2013).
[21]R. J. Ellingson, M. C. Beard, J. C. Johnson, P. Yu, O. I. Micic, A. J. Nozik, A. Shabaev, and A. L. Efros, Nano Lett. **5**, 865 (2005).
[22]I. Robel, V. Subramanian, M. Kuno, and P. V. Kamat, J. Am. Chem. Soc. **128**, 2385 (2006).
[23]C. S. Ponseca, Jr., T. J. Savenije, M. Abdellah, K. Zheng, A. Yartsev, T. Pascher, T. Harlang, P. Chabera, T. Pullerits, A. Stepanov, J. P. Wolf, and V. Sundstrom, J. Am. Chem. Soc. **136**, 5189 (2014).
[24]P. D. Cunningham and L. M. Hayden, J. Phys. Chem. C **112**, 7928 (2008).
[25]Q. Wang, J. E. Moser, and M. Grätzel, J. Phys. Chem. B **109**, 14945 (2005).
[26]J. Bisquert, J. Phys. Chem. B **106**, 325 (2002).
[27]J. van de Lagemaat, N. G. Park, and A. J. Frank, J. Phys. Chem. B **104**, 2044 (2000).
[28]L. Dloczik, O. Ileperuma, I. Lauermann, L. M. Peter, E. A. Ponomarev, G. Redmond, N. J. Shaw, and I. Uhlendorf, J. Phys. Chem. B **101**, 10281 (1997).
[29]R. Pandya and B. A. Khan, J. Appl. Phys. **62**, 3244 (1987).
[30]D. S. Shen and S. Wagner, J. Appl. Phys. **79**, 794 (1996).
[31]J. Gao, A. F. Fidler, and V. I. Klimov, Nat. Commun. **6**, 8185 (2015).
[32]X. Guo, N. Zhou, S. J. Lou, J. Smith, D. B. Tice, J. W. Hennek, R. P. Ortiz, J. T. L. Navarrete, S. Li, J. Strzalka, L. X. Chen, R. P. H. Chang, A. Facchetti, and T. J. Marks, Nat. Photonics **7**, 825 (2013).
[33]P. R. F. Barnes, K. Miettunen, X. Li, A. Y. Anderson, T. Bessho, M. Grätzel, and B. C. O'Regan, Adv. Mater. **25**, 1881 (2013).
[34]B. C. O'Regan and F. Lenzmann, J. Phys. Chem. B **108**, 4342 (2004).
[35]X. Chen and B. Wu, Rev. Sci. Instrum. **86**, 013905 (2015).
[36]H. Diesinger, M. Panahandeh-Fard, Z. Wang, D. Baillargeat, and C. Soci, Rev. Sci. Instrum. **83**, 053103 (2012).
[37]B. C. O'Regan, K. Bakker, J. Kroeze, H. Smit, P. Sommeling, and J. R. Durrant, J. Phys. Chem. B **110**, 17155 (2006).
[38]N. Cai, S. J. Moon, L. Cevey-Ha, T. Moehl, R. Humphry-Baker, P. Wang, S. M. Zakeeruddin, and M. Grätzel, Nano Lett. **11**, 1452 (2011).
[39]H. Zhang, J. Shi, J. Dong, X. Xu, Y. H. Luo, D. M. Li, and Q. B. Meng, J. Energy Chem. **24**, 707 (2015).
[40]J. Shi, X. Xu, D. M. Li, and Q. B. Meng, Small **11**, 2472 (2015).
[41]F. Marlow, A. Hullermann, and L. Messmer, Adv. Mater. **27**, 2447 (2015).
[42]W. Tress, N. Marinova, T. Moehl, S. M. Zakeeruddin, M. K. Nazeerudin, and M. Grätzel, Energy Environ. Sci. **8**, 995 (2015).
[43]J. Wei, Y. Zhao, H. Li, G. Li, J. Pan, D. Xu, Q. Zhao, and D. Yu, J. Phys. Chem. Lett. **5**, 3937 (2014).
[44]Y. Shao, Z. Xiao, C. Bi, Y. Yuan, and J. Huang, Nat. Commun. **5**, 5784 (2014).
[45]H. Zhang, X. Xiao, Y. Shen, and M. Wang, J. Energy Chem. **24**, 729 (2015).
[46]Y. Zhang, Z. Yao, S. Lin, J. Li, and H. Lin, Acta Chim. Sin. **73**, 219 (2015).
[47]J. Shi, X. Xu, H. Zhang, Y. H. Luo, D. M. Li, and Q. B. Meng, Appl. Phys. Lett. **107**, 163901 (2015).
[48]J. Shi, H. Zhang, X. Xu, D. M. Li, Y. H. Luo, and Q. B. Meng, Small **12**, 5288 (2016).
[49]S. W. Kettlitz, J. Mescher, N. S. Christ, M. Nintz, S. Valouch, A. Colsmann, and U. Lemer, IEEE Photonics Technol. Lett. **25**, 682 (2013).